



# Mitigation of Darrieus–Landau instability effects on turbulent premixed flames

Pasquale Eduardo Lapenna<sup>a,b,\*</sup>, Guido Troiani<sup>a</sup>, Rachele Lamioni<sup>b</sup>,  
Francesco Creta<sup>b</sup>

<sup>a</sup> ENEA C.R. Casaccia, via Anguillarese 301, Rome, Italy

<sup>b</sup> Department of Mechanical and Aerospace Engineering, University of Rome "La Sapienza", Italy

Received 7 November 2019; accepted 6 July 2020

Available online xxx

## Abstract

Theoretical considerations on the competition between the most amplified modes for Darrieus–Landau (DL) hydrodynamic instability and turbulence timescales, show that, two extremal regimes can be identified: the instability-dominated and turbulence-dominated regimes. In the latter, also denoted as unified regime, both experiments and numerical simulations give evidence showing how the large scale, cusp-like structures of the flame front surface, typical of DL instability, are hindered by turbulent fluctuations. The result is that quantities such as turbulent flame propagation and front curvature statistics, which in the instability dominated regime are enhanced or modified by the overwhelming presence of hydrodynamic instability, are now mitigated and a unified regime is reached in which the characteristics of DL unstable and stable flame configurations become indistinguishable. In this work we analyze the concealing effects of increasing level of turbulence over the hydrodynamic Darrieus–Landau instability, and we show that, although some global indices such as the skewness of the curvature p.d.f. suggest that a unified regime is reached, others show the persistence of residual differences: in particular, the power spectral density of the flame front curvature. We use both experimental and numerical datasets of stable and unstable (based on linear stability analysis) flames, in conditions ranging from quasi laminar to significantly turbulent regimes.

© 2020 The Combustion Institute. Published by Elsevier Inc. All rights reserved.

**Keywords:** Large scale flames; Darrieus–Landau instability; Turbulent premixed combustion; Flame morphology; Direct numerical simulation

## 1. Introduction

The interactions between turbulent motions and a premixed flame front are usually categorized

by comparing chemical and turbulent time/length-scales and summarized in regime diagrams for premixed turbulent combustion [1–3]. Although regime diagrams can qualitatively represent the main aspects of flame-turbulence interaction, intrinsic flame instabilities, such as hydrodynamic or Darrieus Landau (DL) instabilities [4,5], are invariably neglected. Large-scale flames, however, exhibit

\* Corresponding author.

E-mail addresses: [pasquale.lapenna@uniroma1.it](mailto:pasquale.lapenna@uniroma1.it), [pasquale.lapenna@enea.it](mailto:pasquale.lapenna@enea.it) (P.E. Lapenna).

<https://doi.org/10.1016/j.proci.2020.07.018>

1540-7489 © 2020 The Combustion Institute. Published by Elsevier Inc. All rights reserved.

an additional thermochemical lengthscale, which should be considered on an equal footing with other significant lengthscales, namely the neutral or cut-off scale  $\lambda_c$  for which DL instability is balanced by stabilizing diffusive effects [6]. As a result, DL instability can develop for large scale flames, larger than  $\lambda_c$  and be inhibited otherwise. In other words, premixed flames can develop unstable structures in a range of scales bounded between the lower viscous cut-off  $\lambda_c$  and a reference hydrodynamic large scale  $L$ . In recent numerical and experimental work [7–9] the hydrodynamic length scale  $L$  is addressed as the experimental device size or numerical domain size, which inherently represents the largest hydrodynamic length scale to which the flame is subjected.

In a laminar scenario, intrinsic instabilities are clearly manifested in the form of a severe large scale cusp-like corrugation of the flame front in the case of purely DL unstable flames. When thermal-diffusive (TD) effects are destabilizing, a case not addressed explicitly in the present study, an additional small scale corrugation can develop. Conversely, in those cases where an interplay between hydrodynamic instability and turbulent fluctuations does exist, the situation is significantly more complex, as illustrated in many theoretical studies based on spectral formulations [10,11], renormalization analysis [12–14] and perturbed Sivashinsky equation [15]. This scenario has been recently discussed in [16] as confined between two extremal regimes called *turbulence dominated* and *instability dominated*. Being turbulence a multiscale phenomenon, the flame front is wrinkled in a range of scales also bounded between a large scale (ideally of the same order of the DL instability) and a small dissipative Kolmogorov scale  $\eta$ . For sufficiently high Reynolds numbers, this bounded range corresponds to the inertial range. Some of such scales could indeed match the most amplified scales, defined according to the dispersion relation of DL instability. In the definition of *instability dominated* and *turbulence dominated or unified* regimes, the balance between the time scale in which the most hydrodynamically unstable mode develops and the turbulent time scale associated with the energy containing eddy at that velocity and length scale is considered. It follows that as the Reynolds number increases the energy contained in a given eddy raises together with its representative velocity, at that scale. Hence, if on one hand turbulence can trigger an unstable mode and cause hydrodynamic instability to grow, on the other an excessive energized eddy can distort the flame front according to its eddy turn-over time, depleting and hindering the effects of surface growth induced by DL [17,18].

The trace of residual hydrodynamic instability over a turbulent flame front has been quantified using the skewness of front curvature probability density function in [19]. Negative values of

skewness are found for unstable flames in contrast to stable flames whose skewness values remain small. Recent results seem to confirm the hypothesis according to which, when moving towards a turbulence-dominated regime, a unified behavior can be reached in which skewness values as well as turbulent combustion velocities of DL stable and unstable flames become indistinguishable. This regime, however, was never fully investigated in dedicated experiments. An alternative picture of such turbulence dominated regime, in which the typical DL morphology is effectively concealed by turbulence, can be given by the concept of turbulence-induced cut-off scale which was introduced by the spectral formulation of Chaudhuri et al. [10] also discussed in [11]. Rather than an overpowering of DL front wrinkling under the action of turbulence, it is suggested that as turbulence intensity increases, the turbulence-induced cut-off scale increases accordingly, thus mitigating the development of instability and relegating it to larger and larger scales.

In this work, we perform targeted experiments of DL stable/unstable propane-air Bunsen flames, extending the range of previously investigated Reynolds numbers to higher values so as to encompass a highly turbulent regime where turbulence is expected to dominate over instability effects. Two Bunsen diameters are chosen so as to fall below and above the estimated cut-off value, thus giving rise to a set of stable and unstable flames respectively. In order to further support the experimental findings we also perform direct numerical simulation (DNS) of two slot flames, namely a small and large scale case, increasing the turbulence intensity of a recently developed dataset [8]. The main goal of this work is to focus on the transition from the instability-dominated to the turbulence-dominated regime, detecting and identifying the possible occurrence of such unified regime using statistical and spectral characterization of curvature as well as monitoring global flame features related to turbulence flame propagation.

## 2. Methodology and datasets

### 2.1. Experiments

In order to investigate the mitigation of DL effects we add data at higher Reynolds number ( $Re = 10000$ ) to a previously developed experimental dataset [19] in which two propane-air Bunsen burners with different diameters are used to either promote or suppress the instability. The two diameters employed are 9 mm and 18 mm, respectively yielding DL stable and unstable flames based on a cut-off length  $\lambda_c$  which is intermediate between the two. In the range of equivalence ratios  $\phi$  chosen for the utilized propane-air mixture, the cut-off scale does not vary substantially and for a stoichiometric

Table 1

Velocity corresponding to unreactive cases ( $\phi = 0$ ) expressed in  $\text{ms}^{-1}$ . Mean of the axial velocity  $U_{CL}$  and its root mean square  $u'_0$ , calculated at the centerline, away from the wall boundary layer influence.

Re	D = 9 mm		D = 18 mm	
	$U_{CL}$	$u'_0$	$U_{CL}$	$u'_0$
2500	5.2	0.1	3.2	0.19
5000	9.8	0.5	5.9	0.6
7000	13.4	1.1	6.8	1.0
10000	19.5	1.8	11.8	1.4

mixture is estimated, using available linear stability analysis tools [20], as  $\lambda_c \sim 164l_d \sim 12 \text{ mm}$  [7], where  $l_d$  is the flame thickness, conventionally defined as the thermal diffusivity to the laminar flame speed ratio,  $l_d = D_{th}/S_L$ . In the considered conditions, thermal-diffusive effects are stabilizing, since the Lewis numbers  $Le$  has been estimated in the range  $Le=1.35-1.8$  as reported in [21]. The latter values also explain the elevated ratio between  $\lambda_c$  and  $l_d$  which increases with  $Le$ . The dataset thus features stable and unstable Bunsen flames with Reynolds numbers ranging between 2500 and 10,000, the Reynolds being based on the mixture mass flow rate  $\dot{m}$ , dynamic viscosity  $\mu$ , and the Bunsen diameter  $D$ , i.e.  $Re = 4\dot{m}/\pi\mu D$ .

Particle Image Velocimetry (PIV) is used to probe velocity fields in a diametral plane feeding the reactive mixture with alumina tracers. The flame front position is then determined from the abrupt jump in particle number density, caused by the steep temperature gradient across the front, which corresponds, in Mie scattering images, to regions with rather different intensity of scattered light. For the sake of readiness of images, colors are inverted so that darker zones correspond to reactants and lighter ones to combustion products. Global quantities (i.e. flame surface area under an axis-symmetric flame hypothesis) and local quantities (i.e. flame curvature) are obtained by post-processing the obtained images. Detailed descriptions of the experimental setup and methods can be found in [21–23] while a brief summary of the turbulence intensities is reported in Table 1.

A summary of the experimental dataset is displayed in Fig. 1. For each Reynolds ( $Re$ ) and equivalence ratio ( $\phi$ ), two figures are shown, the left one being the  $D = 18 \text{ mm}$  Bunsen flame (unstable case) while the right one is the  $D = 9 \text{ mm}$  Bunsen flame (stable case). From a first, visual inspection of the flame morphology, differences can be appreciated at low- $Re$  between the two Bunsen diameters. In fact, the characteristic cusp-like structures of DL instabilities are visible only for the unstable case as expected in the *instability dominated regime* [16]. As Reynolds numbers increase, stronger velocity fluctuations and shear layer instability effects tend to mitigate such differences. However, although less

evident, some morphological differences between the two cases are still apparently persist at  $Re = 10000$ .

## 2.2. Direct numerical simulations

In order to support the experimental results, two direct numerical simulations are performed at higher turbulence intensity in order to investigate the effect of increasing velocity fluctuations on DL unstable flames. Such simulations are used to increase the parameter range of a recent DNS dataset [8] developed to investigate relevant features of large scale flames by comparing it with their small scale counterpart. The original dataset comprises four low- $Ka$  simulations labelled as a small/large scale slot Bunsen flame (SB, LB) and small/large scale planar flame (SP, LP). In the entire dataset, TD instability effects are inhibited by selecting  $Le = 1.2$ . In this work we employ only the slot configuration and the new simulations are labelled as SB2 and LB2. They feature identical slot configuration, parameters, computational domain and grid sizes of the SB and LB cases [8]. The only parameter varied is the intensity of the homogeneous isotropic turbulence (HIT) perturbation imposed at the inlet  $u_{rms}/S_L^0 = 2.2$  (1.1 for LB e SB cases) keeping constant the integral lengthscale  $\ell_0 = 0.1L$ , being  $L$  the slot width. Simulations were performed using a well-established DNS framework [7,8,19,24,25] implemented in an equation-of-state-independent version [26–30] of the massively parallel, spectral element, code *nek5000* [31].

## 3. Results and discussion

### 3.1. Re-effects on flame morphology

The morphological features of the flames shown in Fig. 1 are now statistically investigated by means of the probability density function p.d.f. of the flame curvature  $\kappa$ . Figure 2 shows for each  $Re$ , a comparison between the curvature p.d.f.s of the two burner diameters using three representative  $\phi$ 's for each case in order to reduce the additional complexity due to the stretch effect. As the Reynolds increases, the p.d.f.s of the stable case become symmetrically wider, as expected from the wrinkling induced by turbulence. Only at high Reynolds number, such p.d.f.s start to be mildly skewed toward the negative side. Such slight asymmetry can be tentatively considered as the trace of the Huygens corner formation effect. On the other hand, the p.d.f.s of the unstable case show that the main effect of the increasing turbulent fluctuations is a widening of the positive tail. The negative tail of the p.d.f.s remain essentially unaltered as it can be considered to be dominated by the DL-induced wrinkling. As a result, the skewness of the p.d.f.s is reduced as  $Re$  increases. The mixture ratio, irrespectively of the

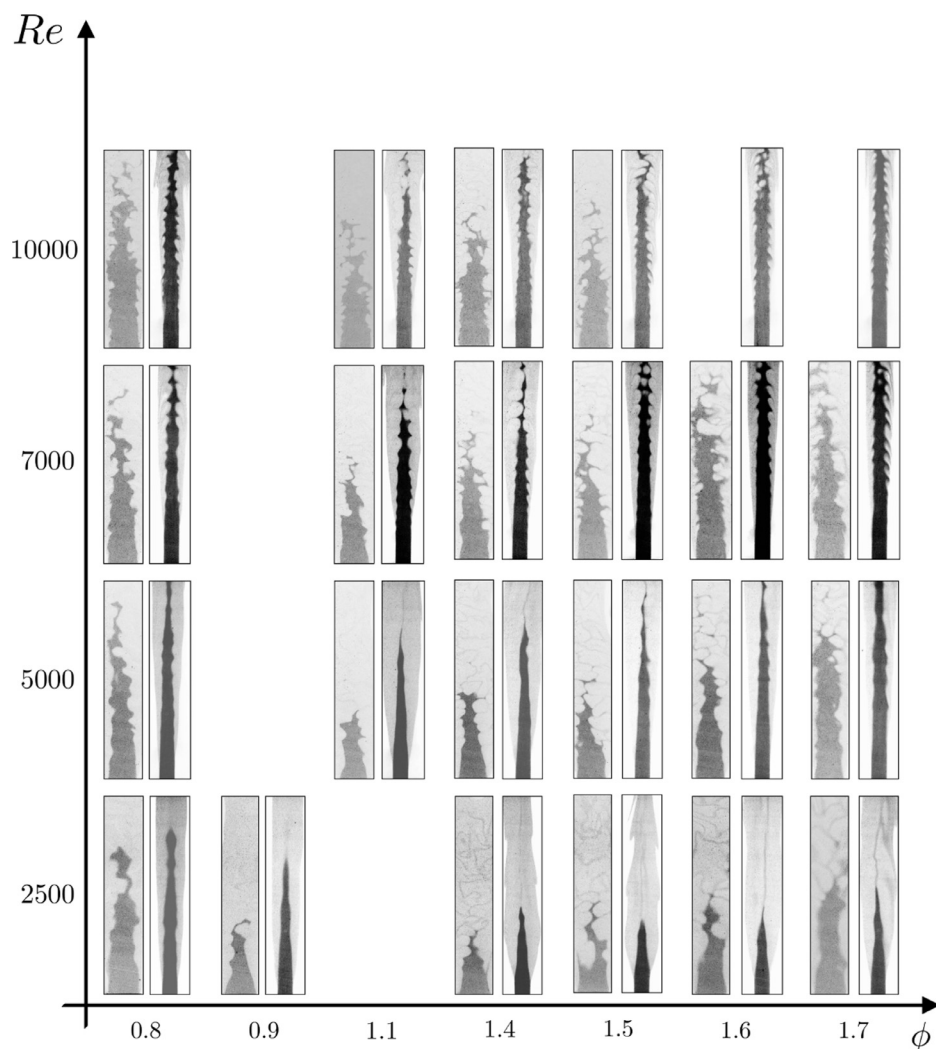


Fig. 1. Summary of the experimental dataset: flames at different Reynolds numbers, equivalence ratios and diameters. For each pair of flames, the left one is within  $D = 18$  mm burner and the right one the  $D = 9$  mm burner.

Reynolds number, is shown to have a limited impact on the p.d.f.s of both the large and small burners.

Following [19], the skewness of the flame curvature p.d.f. is calculated for each new case at high Reynolds number. Figure 3 shows the values of skew( $\kappa$ ) as a function of  $\phi$  for each case and each  $Re$ . Such values, while being constantly negative, decrease as the Reynolds number increases and as  $Re = 10000$  is reached the differences between the stable and unstable cases become minimal. This suggests that DL effects begin to be overshadowed by turbulence and their impact on the flame morphology is thus mitigated. This scenario is also clearly evidenced for three representative values of  $\phi$  in Fig. 4, in which it is evident that the skewness as a marker for DL instability is reaching uniform

values at high  $Re$ . Note that, although having similar skew( $\kappa$ ) values, the overall p.d.f. shape remains rather different as shown in Fig. 2(d).

A similar scenario can be observed in the context of DNS data. Figure 5 shows the p.d.f.s of mean curvature  $K_M$ , defined as  $K_M = (\kappa_1 + \kappa_2)/2$  being  $\kappa_{1,2}$  the principal components of the curvature [32], conditioned to  $c^* = 0.64$  as done in [8]. Consistently with well-known literature results [33], the most probable value of the p.d.f. is around zero for all the cases, irrespectively of the presence of instability and turbulence intensity. For the small-scale flames, the increasing turbulence intensity tends to widen both tails of the p.d.f., in a symmetrical fashion. Conversely, for the large-scale flames, only the positive tail of the p.d.f. is widened

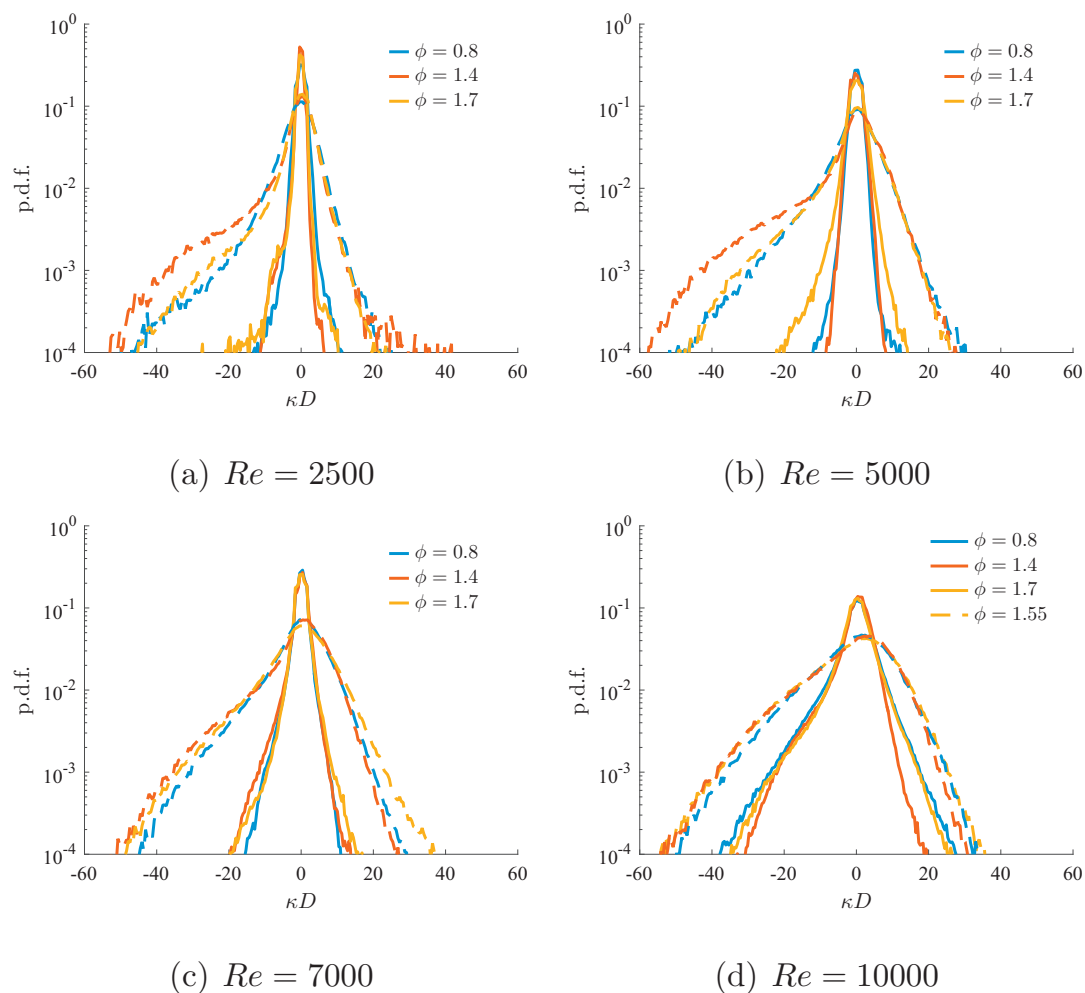


Fig. 2. Curvature p.d.f. at increasing Reynolds number and equivalence ratio for the unstable  $D = 18$  mm case (dashed line) and the stable  $D = 9$  mm case (continuous line) using three representative  $\phi$  values:  $\phi = 0.8, 1.4, 1.7$ . Note that for the higher Reynolds case  $\phi = 1.55$  is reported instead of  $\phi = 1.7$  for the unstable case.

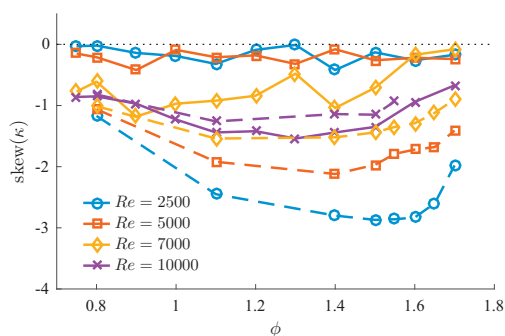


Fig. 3. Skewness of flame curvature p.d.f.'s as a function of the mixture ratio: DL unstable case  $D = 18$  mm (dashed line) and DL stable  $D = 9$  mm cases (continuous line).

while the negative tail remains essentially unaltered. As a result the skewness of such distribution is sensibly reduced. In fact, the skewness values are modified by the increasing turbulence intensity for both the large and small scale flames. In particular, for the LB flame the value is negative, being skew( $K_M$ ) =  $-1.09$ , while an almost null value, skew( $K_M$ ) =  $0.01$ , is obtained for the LB2 case. On the other hand, for the small scale flame we obtain skew( $K_M$ ) =  $-0.46, 0.10$  respectively for SB and SB2. As a result, the instability marker is essentially indicating a complete overshadowing of the instability effect on the flames morphology. Nevertheless, consistently with the experiments at high Reynolds, some differences as shown in Fig. 5 are still present.

The described flame morphologies induced by the DL instability are typically associated with an area increase that directly impacts the turbulent

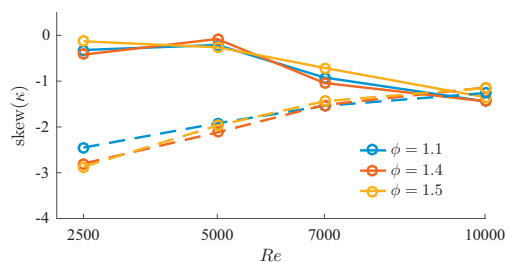


Fig. 4. Skewness of flame curvature p.d.f.'s as a function of the Reynolds number for three representative  $\phi$ : DL unstable case  $D = 18$  mm (dashed line) and DL stable  $D = 9$  mm cases (continuous line).

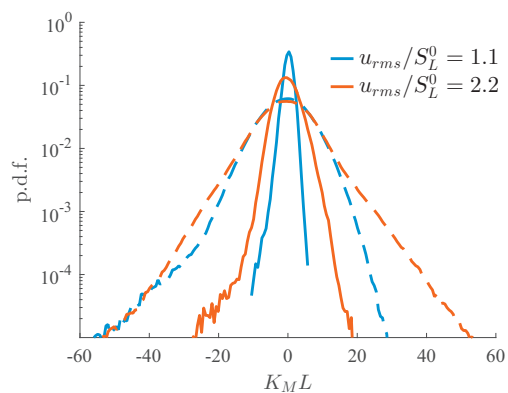


Fig. 5. P.d.f. of the mean curvature  $K_M$  for the DNS cases, large-scale unstable flames (dashed line) and small-scale stable cases (continuous line).

propagation speed, increasing it and giving rise to the so-called DL-enhancement [34]. Simulations have shown that this enhancement, more evident in 2D configurations than in 3D settings [8], is expected to be gradually reduced as turbulence intensity increases. This is indeed the case comparing the global consumption speed of the LB2 and SB2. As usually done for envelope flames [35], the global consumption speed is defined as  $S_{T,GC} = \dot{m} / \rho_u A_{\bar{c}=c^*}$ , being  $\dot{m}$  the slot inlet mass flow rate,  $A_{\bar{c}=c^*}$  the area of the averaged progress variable iso-contour  $\bar{c} = c^*$  and  $\rho_u$  the density of the fresh mixture. The resulting  $S_{T,GC}$  for the LB2 case is lower than SB2, respectively 1.3 and 1.5 times the laminar flame speed, clearly indicating that the DL-enhancement has been completely overshadowed by the incoming turbulence. Note that the SB2 is faster since, although large and small scale flames have been supplied the same HIT at the inflow, the shorter path to the flame of the incoming eddies results in a smaller dissipation for the SB2 case.

On the experimental side, Fig. 6 shows for the  $\phi = 1.4$  case the global consumption speed as a function of  $Re$ . Conversely to the DNS case, the

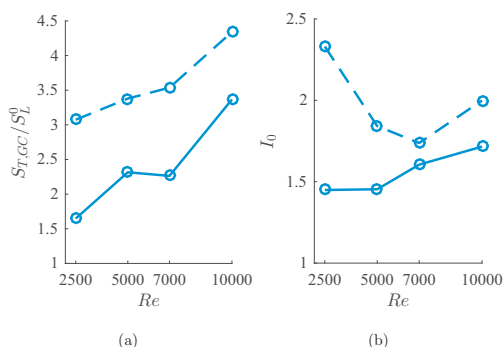


Fig. 6. Reynolds effects on global consumption speed  $S_{T,GC}/S_L^0$  and stretch factor  $I_0$  at equivalence ratio  $\phi = 1.4$  for all conditions: DL unstable case  $D = 18$  mm (dashed line) and DL stable  $D = 9$  mm cases (continuous line).

DL-enhancement is still present at elevated turbulence intensity although being clearly reduced. Figure 6 also displays the stretch factor  $I_0$ , following the operative definition  $S_{T,GC}/S_L^0 = I_0 A_T / A_S$  where  $A_T$  is the turbulent flame area (calculated as the integral of flame surface density over the flame volume) and  $A_S$  the average flame surface. A completely unified regime dominated by turbulence, although being possibly indicated by the skewness marker is not completely achieved at  $Re = 10,000$  neither in terms  $S_{T,GC}/S_L^0$  nor for  $I_0$  suggesting a more detailed analysis of the flame morphology may be required.

### 3.2. Flame curvature power spectral density

As previously shown, at high  $Re$  the skewness marker would suggest the attainment of the unified regime. However, in particular for the experimental dataset, other global flame properties related to the turbulent flame propagation, are still indicating residual differences between the stable and unstable cases. Given that some morphological differences still persist at elevated  $Re$ , the flame curvature distribution along the flame front is additionally investigated in the wave number domain. Operatively a fast Fourier transform algorithm (FFT) is applied to the curvature signal along a curvilinear abscissa, in order to evaluate the power spectral density (PSD). This is repeated for each of the 400 experimental images recorded every  $\phi - Re$  pair and then averaged. A Fourier analysis cannot distinguish between occurrences of negative or positive curvatures, where high negative values are typical for DL instability. Nonetheless, signs of hydrodynamic instability are expected at large scales, indicative of peak-to-peak distances between cusp-like structure.

Figure 7 shows the PSD of the flame curvature signal for Reynolds numbers 5000, 7000 and

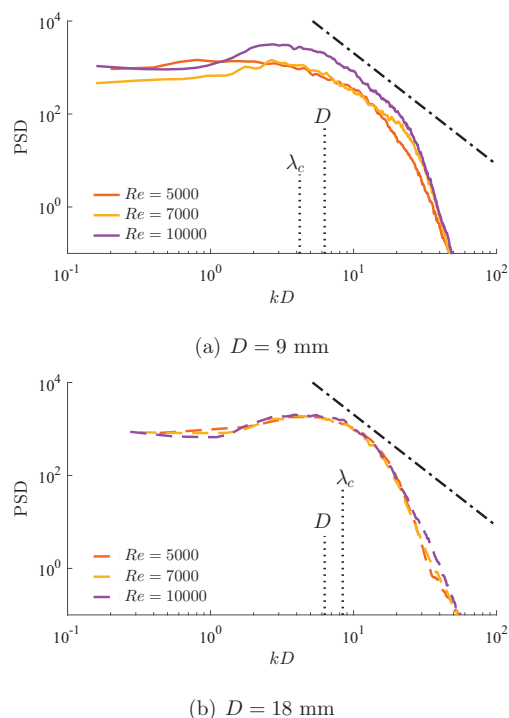


Fig. 7. Power spectral density of the flame curvature signal for the small stable (a) and large unstable (b) Bunsen burners at  $\phi = 1.4$ . The black dotted line indicate the scaling law  $kD^{-2.4}$  reported in [36].

10,000 with wavenumbers  $k$  normalized with the Bunsen diameter  $D$ . Since the curvature signal at the lower Reynolds number of 2500 is only mildly fluctuating, the corresponding spectrum is not shown. The wavenumber corresponding to the diameter,  $kD = 2\pi$  and the estimated cut-off scale,  $\lambda = \lambda_c$ , are also displayed for both the stable and unstable cases. In the stable case, as  $Re$  increases the PSD approaches a  $-2.4$  scaling at intermediate wavenumbers in accordance with results found elsewhere [36]. On the other hand, when DL instability is induced in the larger Bunsen, the cut-off scale wavenumber falls on the right side of the wavenumber corresponding to the burner diameter. Between those two scales, the DL dispersion relation exhibits positive growth rates, the system being DL unstable and the flame front wrinkling altered by the action of the cusp-like structures. No distinct peaks of the PSD that can be directly related to DL instability are observed, although it modifies the behavior of finer, front curvature scales thus inhibiting the onset of the scaling law found for the stable case. Indeed, the PSD of the  $D = 18$  mm case appears to be insensitive to the increasing  $Re$  and does not show any apparent tendency to exhibit the  $-2.4$  scaling at higher  $Re$ .

#### 4. Conclusion

Targeted premixed flame experiments and direct numerical simulations were performed with the objective of investigating the transition from the DL instability-dominated to the turbulence-dominated regime. Experiments of DL stable/unstable propane-air Bunsen flames have shown that as the  $Re$  increases, the DL-induced morphological features are mitigated. The flame curvature statistics was investigated at increasing  $Re$  numbers and converging values of the skewness of the p.d.f were observed between the  $D = 18$  mm and  $D = 9$  mm burners. This scenario was confirmed by the statistical analysis of the mean curvature obtained by DNS simulation of small and large scale flames. Although the skewness of the curvature p.d.f. may indicate this, a completely unified regime dominated by turbulence cannot be considered to have been fully achieved at  $Re = 10,000$  since difference in terms of both the global consumption speed and stretch factor are observed to persist. Finally, a more detailed analysis of the flame curvature, by means of the power spectral density, has confirmed the persistence of residual morphological differences between the stable and unstable case.

#### Declaration of Competing Interest

None.

#### Acknowledgments

The authors acknowledge CINECA for computing resources (IscRB-DNS-LS grant).

#### References

- [1] N. Peters, *Jour. Fluid Mech.* 384 (1999) 107–132.
- [2] N. Peters, *Turbulent Combustion*, Cambridge University press, UK, 2000.
- [3] A. Lipatnikov, J. Chomiak, *Progr. in Energ. Combust. Sci.* 36 (1) (2010) 1–102.
- [4] G. Darrieus, 1938. *Unpublished work*; presented at La Technique Moderne (Paris) and in 1945 at Congrès de Mécanique Appliquée.
- [5] L. Landau, *Acta Phys. Chim. USSR* 19 (1944) 77–85.
- [6] M. Matalon, *Annu. Rev. Fluid Mech.* 39 (2007) 163–191.
- [7] R. Lamioni, P.E. Lapenna, G. Troiani, F. Creta, *Proc. Combust. Inst.* 37 (2) (2019) 1815–1822.
- [8] P.E. Lapenna, R. Lamioni, G. Troiani, F. Creta, *Proc. Combust. Inst.* 37 (2) (2019) 1945–1952.
- [9] E. Al Sarraf, C. Almarcha, J. Quinard, B. Radisson, B. Denet, P. Garcia-Ybarra, *Proc. Combust. Inst.* 37 (2) (2019) 1783–1789.
- [10] S. Chaudhuri, V. Akkerman, C.K. Law, *Phys. Rev. E* 84 (2) (2011) 026322.

- [11] V. Akkerman, S. Chaudhuri, C.K. Law, *Phys. Rev. E* 87 (2) (2013) 023008.
- [12] V. Bychkov, *Phys. Rev. E* 68 (6) (2003) 066304.
- [13] V. Akkerman, V. Bychkov, *Combust. Theory Model.* 7 (4) (2003) 767–794.
- [14] V. Akkerman, V. Bychkov, *Combust. Theor. Model.* 9 (2) (2005) 323–351.
- [15] F. Creta, N. Fogla, M. Matalon, *Combust. Theor. Model.* 15 (2) (2011) 267–298.
- [16] S. Yang, A. Saha, Z. Liu, C.K. Law, *J. Fluid Mech.* 850 (2018) 784–802.
- [17] H. Kobayashi, H. Kawazoe, *Proc. Combust. Inst.* 28 (1) (2000) 375–382.
- [18] D. Bradley, M. Lawes, K. Liu, M.S. Mansour, *Proc. Combust. Inst.* 34 (1) (2013) 1519–1526.
- [19] F. Creta, R. Lamioni, P.E. Lapenna, G. Troiani, *Phys. Rev. E* 94 (5) (2016) 053102.
- [20] M. Matalon, C. Cui, J. Bechtold, *J. Fluid Mech.* 487 (2003) 179–210.
- [21] G. Troiani, F. Creta, M. Matalon, *Proc. Combust. Inst.* 35 (2) (2015) 1451–1459.
- [22] G. Troiani, M. Marrocco, S. Giammartini, C. Casciola, *Combust. Flame* 156 (3) (2009) 608–620.
- [23] G. Troiani, *Combust. Flame* 156 (2) (2009) 539–542.
- [24] R. Lamioni, P.E. Lapenna, G. Troiani, F. Creta, *Flow Turb. Combust.* 101 (4) (2018) 1137–1155.
- [25] F. Creta, P.E. Lapenna, R. Lamioni, N. Fogla, M. Matalon, *Combust. Flame* 216 (2020) 256–270.
- [26] P.E. Lapenna, F. Creta, *Jour. Supercrit. Fluids* 128 (2017) 263–278.
- [27] P.E. Lapenna, R. Lamioni, P.P. Ciottoli, F. Creta, *AIAA-paper 2018-0346* (2018).
- [28] P.E. Lapenna, *Phys. Fluids* 30 (7) (2018) 077106.
- [29] P.E. Lapenna, F. Creta, *AIAA J.* 57 (6) (2019) 2254–2263.
- [30] P.E. Lapenna, G. Indelicato, R. Lamioni, F. Creta, *Acta Astronaut.* 158 (2019) 460–469.
- [31] P.F. Fischer, J.W. Lottes, S.G. Kerkemeier, <http://nek5000.mcs.anl.gov>(2008).
- [32] S. Pope, P. Yeung, S. Girimaji, *Phys. Fluids A: Fluid Dynamics* 1 (12) (1989) 2010–2018.
- [33] T. Poinsot, D. Veynante, *Theoretical and Numerical Combustion*, RT Edwards, Inc., 2005.
- [34] F. Creta, M. Matalon, *J. Fluid Mech.* 680 (2011) 225–264.
- [35] J.F. Driscoll, *Progr. Energy Combust. Sci.* 34 (1) (2008) 91–134.
- [36] S. Kheirkhah, Ö. Gülder, *Phys. Fluids* 25 (5) (2013) 055107.